Available online at www.sciencedirect.com
SCIENCE DIRECT®
Polymer 44 (2003) 6397–6405
polymer
www.elsevier.com/locate/polymer

Spatial distribution of lamella structure in PCL/PVB band spherulite investigated with microbeam small- and wide-angle X-ray scattering

Yoshinobu Nozue[a,*], Rei Kurita[a], Satomi Hirano[a], Naohiko Kawasaki[b], Satoru Ueno[c], Atsuo Iida[d], Toshio Nishi[a], Yoshiyuki Amemiya[a,b]

[a]*Department of Applied Physics, The University of Tokyo, Hongo, Bunkyo-ku, Tokyo, Japan*
[b]*Department of Advanced Materials Science, The University of Tokyo, Kashiwa, Chiba, Japan*
[c]*Faculty of Applied Biological Science, Hiroshima University, Higashihiroshima, Japan*
[d]*Photon Factory, Institute of Materials Structure Science, High Energy Accelerator Research Organization (KEK), Tsukuba, Japan*

Received 10 January 2003; received in revised form 28 May 2003; accepted 16 June 2003

Abstract

The microbeam small- and wide-angle X-ray scattering (SAXS/WAXS) technique gives the novel information about micron-scale structural inhomogeneity of polymer crystal. By using this technique, we have studied structural inhomogeneity of lamella within the band spherulite of miscible polymer blend poly(ε caprolactone) (PCL)/poly(vinyl butyral) (PVB) and the structure development of lamella during crystallization. It is known that PCL/PVB forms very large spherulites (~several mm in radius) with highly regular band structure because of low frequency of nucleation and that PCL/PVB crystallized at 41 °C has at least two kinds of lamella structure (150 Å, 180 Å). With an X-ray microbeam initially fixed outside near the growth front of the band spherulite, we have observed the lamella formation at the local point and have found that the larger long period grows before the appearance of the shorter long period. We have also observed that the orientation of lamella with the larger long period is different from that of lamella with the shorter long period from SAXS experiment with an X-ray microbeam scanning the band spherulite along its radial direction. Further, the discontinuity in lamella twisting was observed from scanning microbeam WAXS. Based on the experimental results, we propose two possible spatial distribution models. The result of PCL/PVB crystallized at 35 °C was also discussed.

Keywords: Microbeam small-angle X-ray scattering; Poly(ε caprolactone); Poly(vinyl butyral)

1. Introduction

It is known that many polymer blend systems show the micron-scale inhomogeneity in their structures due to the phase separation [1,2], twisting of lamella planes [3,4] and so on. The understanding of structural inhomogeneity in polymer blend will give us precious information about its physical properties such as the strength for mechanical stress and electron conductivity. To obtain the information about the lamella structure, small-angle X-ray scattering (SAXS) technique is a powerful tool and a considerable amount of SAXS experiments for polymer blend systems have been performed. In the usual SAXS experimental setup, the X-ray beam size is about 0.5–2 mm in diameter, which is too large to obtain the micron-scale inhomogeneity of the lamella structure.

Recent development of X-ray focusing optics together with the advent of synchrotron radiation facility has enabled us to make an intense X-ray microbeam which has a low divergence enough to record X-ray scattering at low scattering angles [5]. However, the examples of the application of microbeam SAXS to polymer blend systems are still limited and besides there are few works that thoroughly utilize the merit of microbeam SAXS [6] compared with microbeam wide-angle X-ray scattering (WAXS) [7–10]. We have developed the X-ray optics for microbeam SAXS just by inserting two sets of pinholes into the microbeam focusing X-ray optical system, and have obtained a small angle resolution enough to record X-ray scattering at $s > 0.01$ ($s = 4\pi \sin\theta/\lambda$, θ : Bragg angle).

* Corresponding author. Address: Petrochemicals Research Laboratory, Sumitomo Chemical Co., Ltd, 2-1 Kitasode Sodegaura City, Chiba 299-0125, Japan. Tel.: +81-436-61-5340; fax: +81-436-61-5198.
E-mail address: nozue@sc.sumitomo-chem.co.jp (Y. Nozue).

0032-3861/03/$ - see front matter © 2003 Elsevier Ltd. All rights reserved.
doi:10.1016/S0032-3861(03)00591-3

The purpose of the present study is to observe the lamella structure and its development during crystallization of poly(ε-caprolacton) (PCL)/poly(vinyl butyral) (PVB) band spherulite by applying microbeam SAXS and WAXS. It is known that the PCL/PVB shows the following highly specific behaviors [11,12]: (1) the addition of a small amount of PVB molecules dramatically reduces the rate of the nucleation of PCL spherulite, (2) a PCL/PVB spherulite forms a highly regular banding structure. A previous SAXS study of PCL/PVB band spherulite showed that the PCL/PVB spherulite includes at least two kinds of lamella structures [11]. However, they could not show how these lamella structures were spatially distributed in the band spherulite. Microbeam SAXS is required to obtain the information on the structural inhomogeneity of lamella structure.

In the present study, we have performed the following experiments: (1) time-resolved microbeam SAXS of PCL/PVB during crystallization with an X-ray microbeam, the position of which is initially fixed outside near the growth front of band spherulite to observe the crystal growth at local point, and (2) microbeam-scanning simultaneous SAXS/WAXS to observe the spatial distribution of two kinds of lamellae (SAXS) and the twisting behavior of lamellae (WAXS). Based on the results of these experiments, we have proposed structural models in the band spherulite.

2. Experimental section

2.1. Materials

PCL and PVB were supplied by Polysciences Inc. (Warrington, PA) and were used as received. M_w of PCL was 65,000 and M_w of PVB was 100,000. The PCL/PVB blend ratio used in our experiment was 95/5. The blend sample was prepared by dissolving the desired ratio of PCL and PVB in the common solvent tetrahydrofuran. The solution sample was cast upon a glass plate. After the solvent was removed at room temperature, the sample was kept in vacuum at 80 °C for 1 day and at 41 or 35 °C for 1 week. A small amount of blend film was cut from the glass container, and was put on the thin mica substrate placed on a hot plate to be melted. Finally, it was gently extended by a micro-spartel to be thinned. The thickness of the sample was about 30–50 μm.

2.2. Microbeam SAXS/WAXS measurement

The experiment was made at BL-4A, Photon Factory (KEK, Tsukuba, Japan). The X-ray beam was monochromated at 1.54 Å with a multi-layer mirror. Kirkpatrick–Baez (KB) mirrors were used to make a microbeam with a size of about 4 μm (vertical) × 5 μm (horizontal). The size and position of the microbeam were measured by moving a thin metal wire of 2 μm in diameter across the X-ray microbeam while monitoring the transmitted X-ray intensity with an ionization chamber [13]. To obtain a low-divergent X-ray beam enough for SAXS, we inserted two sets of pinholes between KB mirrors and the sample: one with a 300 μm diameter was placed at the downstream-edge of the KB mirrors and the other with a 18 μm diameter was placed just before the sample. The distance between the downstream-edge of the KB mirrors and the sample was as small as 35 mm. To monitor the sample area on which the microbeam was impinging, a microscope system with an illuminating light was used. The sample was illuminated by the light from downstream and the light transmitted through the sample was reflected with an optical mirror so that the optical image of the sample was obtained with the microscope. The focus distance of microscope lens was around 50 mm. The camera length for microbeam SAXS was 1600 mm. The precise camera length was calibrated with the Silver Behenate diffraction peak of 58.4 Å [14]. We used a LINKAM (THMS-600) as a sample cell, which can control the sample temperature with a rate range of 0.01–130 °C/min. This range of heating/cooling rates was enough to perform a temperature-jump (T-jump) or a temperature-quench (T-quench) experiment. SAXS profile was measured with a cooled CCD coupled with an X-ray Image intensifier (I.I) [15]. For the microbeam simultaneous SAXS/WAXS measurement, imaging plate with a hole of 20 mm diameter at the center was used for WAXS data acquisition. In the crystallization kinetics experiment, the beam position of microbeam was fixed near the growth front of the band spherulite. In the microbeam-scanning SAXS/WAXS experiment, we used a microbeam of 4 μm (in full width of half maximum (FWHM)) and the microbeam scanned the band spherulite along the radial direction with a step of 1 μm.

2.3. Usual SAXS measurement

The experiment was performed at BL-15A, Photon Factory. The beam was focused with a bending mirror and a bending monochromator crystal [16]. The X-ray wavelength was 1.50 Å and the beam size was about 500 μm × 500 μm at a sample position. The camera length was 2300 mm. The diameter of spherulite was around 2–3 mm which was larger than the X-ray beam size. The X-ray beam position was measured by using a microscope system which was similar to that used at BL-4A. For the alignment of the sample into the X-ray beam pass, a thin phosphor screen was placed at the sample position in LINKAM and then the fluorescent light from the phosphor screen was observed with the microscope.

2.4. Calculation of azimuthal distribution of 110 reflection intensities in the scanning WAXS

The azimuthal distribution of intensities of 110 reflection

in WAXS was calculated to interpret the experimental results. The angular spread of 110 lattice in the reciprocal space were approximated with an isotropic Gauss function (whose decay constant was a free parameter) on the sphere shell (see Fig. 1), and the lattice constant used was $a = 7.97$ Å, $b = 4.76$ Å [17]. The electron density of 110 lattice on the sphere shell was calculated along the cross-section with Ewald sphere shell. The dependence of azimuthal distribution of 110 reflection intensities on the lamella rotation was calculated with a continuous and various discontinuous twisting modes to obtain a reasonable twisting model. In this calculation, the convolution effect by the finite beam size (FWHM = 4 μm) was also taken into consideration. However, the lamella structure distribution effect with respect to the thickness direction of the sample (30–50 μm) was ignored because the sampling position of scanning WAXS was more than 200 μm away from the center of the spherulite and the structure distribution effect along the sample thickness was expected to have much smaller contribution than the convolution effect by the finite beam size.

3. Results

3.1. Usual SAXS of pure PCL and PCL/PVB during melting

Fig. 2 shows the melting behaviors of PCL (A) and PCL/PVB (B) spherulite isothermally crystallized at 41 °C observed with usual SAXS measurements. In Fig. 2, SAXS intensities are displayed as contour maps with scattering vector in the abscissa and temperature in the ordinate. Fig. 2(a) shows the increase in long period in pure PCL during the melting. Similar phenomena have been found in many crystalline polymer and considered as the partial melting process of thinner lamella [18]. On the other hand, it is clearly observed that two different components of lamellae in PCL/PVB show different melting behaviors in Fig. 2(b). Although the precedent experiment by other authors also found that there are two different long period components in lamella structures of isothermally crystallized PCL/PVB at the temperature above 35 °C, they did not discuss the difference in the melting behaviors near the melting points. The melting behavior of one component that has a shorter long period, L in PCL/PVB in Fig. 2(b) looks similar to that of pure PCL in Fig. 2(a). This indicates that a shorter L component has a lamella structure similar to that of pure PCL. On the other hand, the other component that has a larger L shows a melting behavior which is quite different from that of a shorter L component: The larger L component has a higher melting temperature than that of the shorter L component (see arrow). Furthermore, the change in the larger L during melting is smaller than that of the shorter L. From this result, it is considered that a shorter L component which has a lamella structure similar to pure PCL, is hardly affected by the addition of PVB molecules, and that the appearance of the larger L component which has a higher thermal stability is related to the addition of PVB molecules.

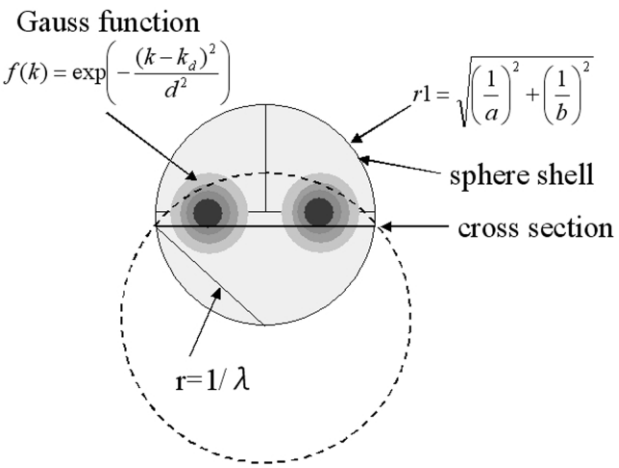

Fig. 1. Polar view of the angular spread of 110 lattice in the reciprocal space. In our model, the angular spread of 110 lattice on the sphere shell is approximated with a Gauss function centered at the peak position k_p with d as a sigma on the sphere-shell. The cross-section of the sphere shell having $r = \sqrt{(1/a^2) + (1/b^2)}$ (shown by thick line) with Ewald sphere shell yields the azimuthal distribution of 110 reflection in WAXS, where a, b are lattice constants of a and b-axes, respectively.

3.2. Time-resolved microbeam SAXS of PCL/PVB during crystallization near the growth front

Fig. 3 shows the change in SAXS profiles of PCL/PVB during isothermal crystallization. The PCL sample melted at 80 °C for 20 min was quenched with a 130 °C/min cooling rate and isothermally crystallized at 41 °C. The exposure time for one frame was 6 s and an interval between the data acquisition was 50 s. The position of the X-ray beam was initially adjusted just outside near the growth front of PCL/PVB band spherulite and was fixed throughout the experiment. It is evident from Fig. 3 that the larger L component of lamella appears in the first stage of crystallization and that the shorter L component of lamella starts to grow in the late stage of crystallization. As previously reported [11], the shoulder at a lower scattering vector (see arrow in Fig. 3) in the scattering profile clearly remains until the end of crystallization, showing that both the larger and shorter components of lamella coexist at the end of crystallization. This means that the structure of the larger component that is formed in the first stage of crystallization is preserved until the late stage of crystallization in the PCL/PVB band spherulite.

3.3. Microbeam-scanning SAXS of PCL/PVB

Fig. 4 shows the change in SAXS intensity profiles from the PCL/PVB band spherulite isothermally crystallized at 41 °C when the X-ray microbeam scans the spherulite along its radial direction at about 200 μm from the center of the

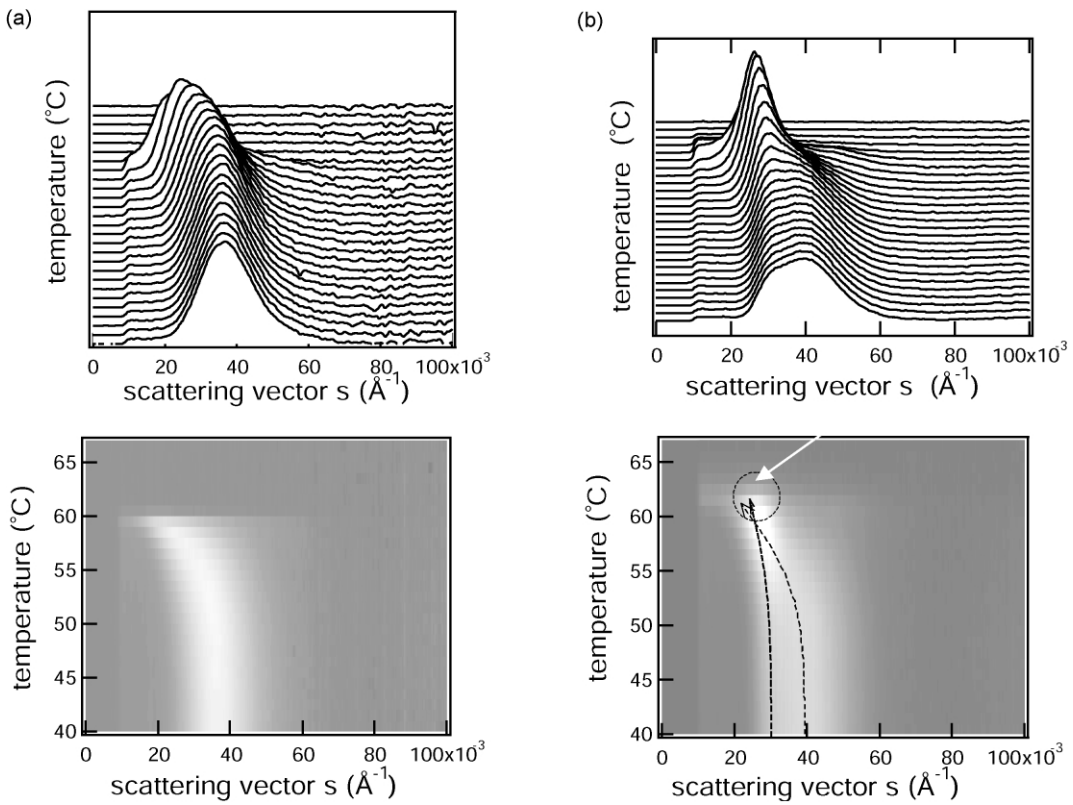

Fig. 2. SAXS intensity contour maps and bird's eye view plots during melting of pure PCL (a) and PCL/PVB (b) isothermally crystallized at 41 °C. The heating rate is 2 °C/min. The scattering vector is taken in the abscissa and temperature in the ordinate. The arrow in (b) shows the difference in thermal stability between two kinds of lamellae, and the dotted lines are drawn for eye guidance.

spherulite. In this region, the sample thickness effect is much smaller than the convolution effect by the beam size of microbeam (FWHM = 4 μm). In Fig. 4, the SAXS intensities are displayed as a contour map with a scanning distance in the ordinate and scattering vector in the abscissa. The scanning step of the microbeam was 1 μm and the exposure time was 6 s for each frame. The data was smoothed and interpolated along the scanning distance to minimize the fluctuation due to X-ray photon statistics. It was found that SAXS intensities changed periodically (data not shown) with a period of 12–14 μm, which correspond to the band period of the spherulite that was observed by a polarized optical microscope (POM). This means that the lamella planes are twisted along the beam-scanning direction, that is, along the radial direction of the spherulies. The marks (+) in Fig. 5 show the peak positions of SAXS

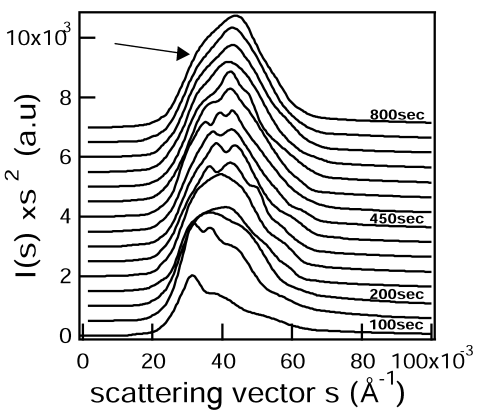

Fig. 3. SAXS profiles of PCL/PVB during crystallization with an X-ray microbeam positioned just outside near the growth front of the band shperulite. See the text about the arrow.

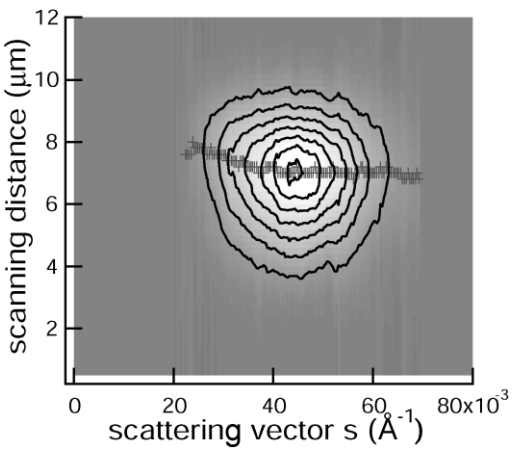

Fig. 4. SAXS intensity contour maps with an X-ray microbeam scanning a PCL/PVB band spherulite (isothermally crystallized at 41 °C) along its radius. Scattering vector is taken in the abscissa and scanning distance in the ordinate. The size of the microbeam in the scanning direction is 4 μm. The step of the scan is 1 μm. Marks (+) indicate the peak position along the scanning direction at respective scattering vectors.

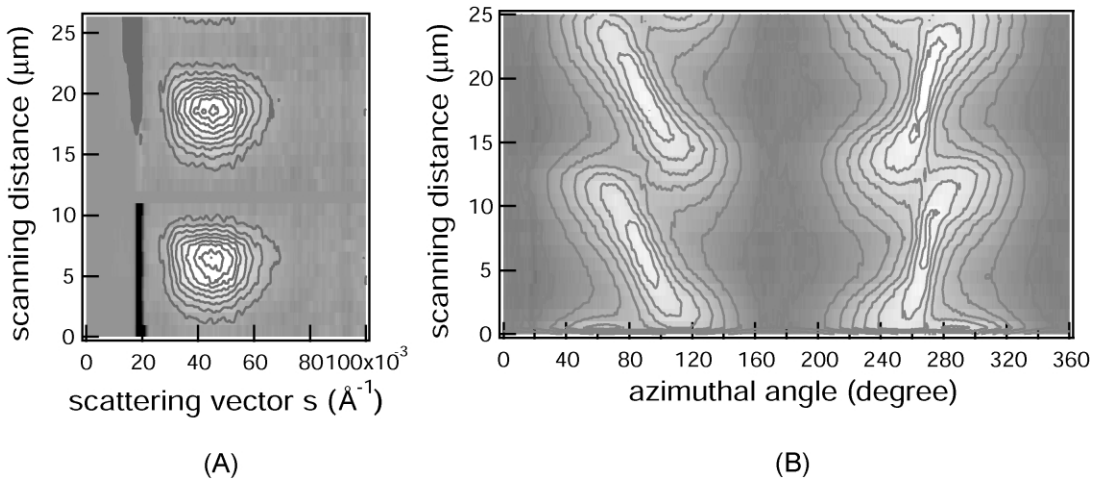

Fig. 5. Intensity contour maps of SAXS (A) and 110 reflection azimuthal distribution from WAXS (B) with an X-ray microbeam scanning the PCL/PVB band spherulite isothermally crystallized at 41 °C along its radius. Azimuthal angle is taken in the abscissa in 110 reflection contour map, whereas scattering angle in SAXS contour map.

intensities along the scanning distance at respective scattering vectors. It is clearly observed that the peak positions at the lower scattering vectors shift by about 1 μm in the beam-scanning direction from those at higher scattering vectors. If all the lamella planes are assumed to be parallel, the peak positions should be aligned straight along the direction of scattering vector, because the difference in Bragg angles for different long periods (~0.1°) are negligible when compared with the difference in the twisting angle of lamellae corresponding to a 1 μm beam scan (~10°) along the beam-scanning direction. Therefore, this result indicates that the lamella planes which have the larger L are not parallel to those that have the shorter L. It should be noted that the SAXS intensity contour is smeared along the beam-scanning direction because of the finite beam size of about 4 μm in FWHM. Nevertheless, the shift in the peak positions in the beam-scanning direction can be still observed. If a beam size could be further reduced, the contour map would be compressed in the beam-scanning direction, enabling us to observe a peak shift more clearly. We have performed the same kind of scanning SAXS experiment for PCL/PVB crystallized at 35 °C and have observed the change in SAXS intensity profile with a single peak (data not shown). In this experiment, the shape of observed SAXS profiles, though the intensity is periodically changed, is almost unchanged during the scanning.

3.4. Scanning SAXS/WAXS of PCL/PVB

In this experiment, we measured scanning SAXS/WAXS for PCL/PVB isothermally crystallized at 35 and 41 °C. The sample condition was same as that for the scanning SAXS experiment except for the exposure time for WAXS (12 s). The SAXS intensities and azimuthal distribution of 110 reflection intensities in WAXS from the band spherulite with a scanning X-ray microbeam are represented as contour maps. The results from PCL/PVB crystallized at 41 and 35 °C are shown in Figs. 5 and 6, respectively. The periodic change in azimuthal distribution of 110 reflection intensities has been observed in the same manner as was previously reported [19,20]. For example, when the lamella plane was parallel to the incident X-ray, SAXS intensity shows the maximum and the 110 reflections show two spots in the contour map. When the incident X-ray was normal to the lamella plane, SAXS intensity becomes minimum and the 110 reflections show four spots in the contour map. When the contour map of azimuthal distribution of Figs. 5 and 6 are compared, they are quite different from each other. In the case of PCL/PVB crystallized at 35 °C (Fig. 6), the intensity of 110 reflections becomes maximum in the region of the scanning distance where four spots are observed. On the other hand, in the case of PCL/PVB crystallized at 41 °C, it becomes maximum in the region of the scanning distance where two spots are observed. The difference in 110 reflection intensity between PCL/PVB crystallized at 35 and 41 °C will indicate the difference in twisting structure.

Discussion on the azimuthal distribution of 110 reflection intensities in the contour map will be made in Section 4.

4. Discussion

To summarize the experimental results above:

(1) During the isothermal crystallization of PCL/PVB at 41 °C, the lamella with the larger L is formed prior to that with the shorter L.
(2) The orientation of the lamella plane with the larger L is different from that of the lamella plane with the shorter L in PCL/PVB crystallized at 41 °C.
(3) The melting behavior of the lamella with the shorter L in PCL/PVB isothermally crystallized at 41 °C looks similar to that of the lamella in pure PCL isothermally

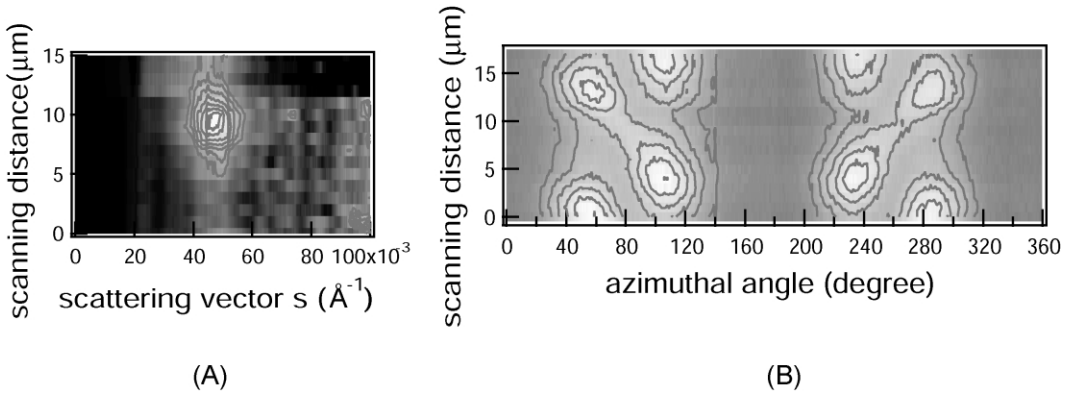

Fig. 6. SAXS (A) and 110 reflection azimuthal distribution from WAXS (B) intensity contour maps with an X-ray microbeam scanning PCL/PVB band spherulite isothermally crystallized at 35 °C.

crystallized at 41 °C. On the other hand, the lamella with the larger L seems to have a higher melting temperature than that with the shorter L in PCL/PVB.

(4) From scanning SAXS/WAXS, the twisting structures between PCL/PVB crystallized at 35 °C seems different from that at 41 °C.

Based on these experimental results, we discuss the structure of the banded spherulite in detail.

4.1. Twisting manner of lamella

In order to interpret the periodic change in azimuthal distribution of 110 reflection intensities obtained from the scanning WAXS experiment, we have simulated contour maps of 110 reflection intensities based on continuous and discontinuous twisting models. The continuous twisting model assumes that the lamella plane is twisted with a single twisting rate along the radius of the spherulite, whereas the discontinuous twisting model assumes that the lamella plane is twisted with two twisting rates (fast and slow twisting rates). The calculated 110 reflection contour map based on the continuous twisting model is shown in Fig. 7(A). In this model, the scattering intensities of 110 reflections show the maximum in the region of the scanning distance where four 110 reflections are observed. The shape shown in Fig. 7(A) is similar to the experimental result from PCL/PVB crystallized at 35 °C (Fig. 6(B)). This means that the lamella is twisted continuously in PCL/PVB crystallized at 35 °C. To mimic the contour map of 110 intensities obtained from PCL/PVB crystallized at 41 °C (Fig. 5(B)), we have made simulation based on several discontinuous twisting models. We have found that the contour map (Fig. 7(B)) similar to the experimental result is given by the model shown in Fig. 8. In this discontinuous model, the twisting mode has a repetition of slow and fast twistings. In Fig. 8, the rate of slow twisting is about 7.5°/μm and the rate of fast twisting is about 30°/μm when the one period of twisting is supposed as 12 μm. Because the twisting rate in the region where SAXS profile appeared is estimated as about 7.5°/μm, it can be estimated that the angle between the larger and the shorter long periodic lamella plane is about 7–8°. The FWHM of Gauss function, the free parameter that expresses the angular spread of 110 reflection in reciprocal space, used in the discontinuous twisting model is about 35°, which is larger than that of the continuous twisting model (about 28°) in Fig. 7(A). It indicates that the orientation of lamella plane was more broadly distributed in PCL/PVB crystallized at 41 °C compared with PCL/PVB crystallized at 35 °C. It is

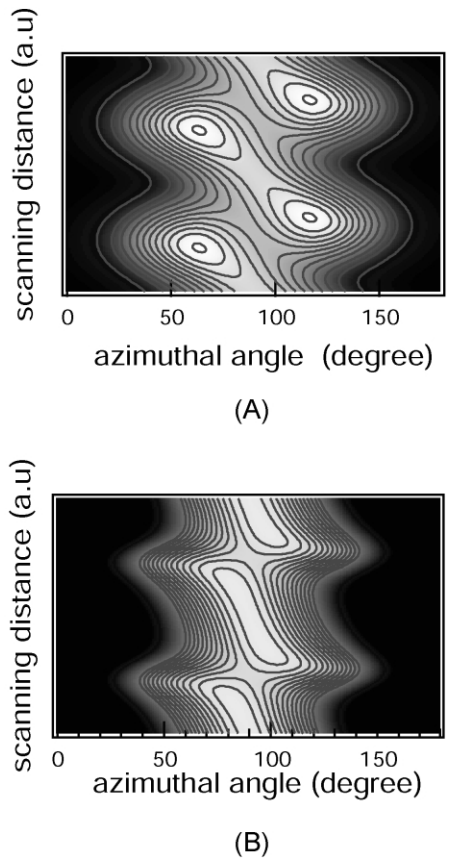

Fig. 7. Simulated intensity contour map of 110 reflection azimuthal distribution along the radial direction. (A) A continuous twisting model, (B) the step-like twisting model shown in Fig. 8.

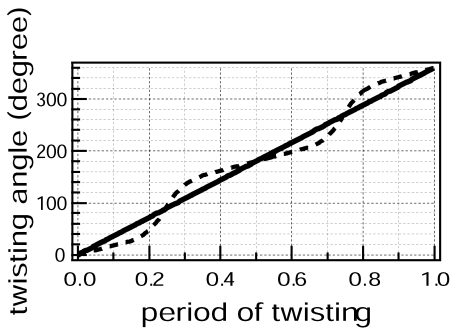

Fig. 8. The behavior of lamella twisting in one band period in the continuous twisting model (solid line) and in the step-like twisting model (dotted line) that was used for the calculation of Fig. 7(B).

worth emphasizing that the scanning microbeam WAXS combined with model calculation will be an useful tool to obtain the information about the twisting manner of lamella.

4.2. Spatial distribution models

Based on the experimental results described above, we propose two possible models about the spatial distribution of the lamella structure with two different long periods. One model is *a parent–daughter lamellae correlation model* (Fig. 9(A)), and the second one is *a S-shaped spatial distribution model* (Fig. 9(B)).

At first, we describe the parent–daughter lamellae correlation model. In this model, the twisting manner of parent and daughter lamellae has some correlation. The daughter lamella will originate from the branching of the parent lamella, and further, the lamella thickness of daughter lamella is thinner than that of parent lamella. In this model, the crystalline thickness of daughter lamella is not affected by PVB and almost same with that of pure PCL. It may indicate that the twisting mechanism of daughter lamella is quite different from that of primary lamella. For example, the driving force of primary lamella may be the strain caused by the attachment of PVB at the radial growth front, and that of daughter lamella may be the strain by the restricted space. If there are some kinds of constant relationship between primary and daughter lamellae such as physical contact at the branching point and restriction of the space for the crystal growth, the correlation of twistings and the relationship of plane angles between primary and daughter lamellae will be kept.

Second, we describe the S-shaped spatial distribution model. In this model, it is supposed that so-called 'S-shaped' lamella model that was already reported in polyethylene [21] can be applied to the banded structure in PCL/PVB crystallized at 41 °C. The S-shaped cross-section of lamella plane in the banded spherulite has been theoretically proposed [22,23] and observed with TEM experiments [24]. The S-shaped spatial distribution model which we propose here means that there is inhomogeneity of lamella long period in the S-shaped lamella cross-section of

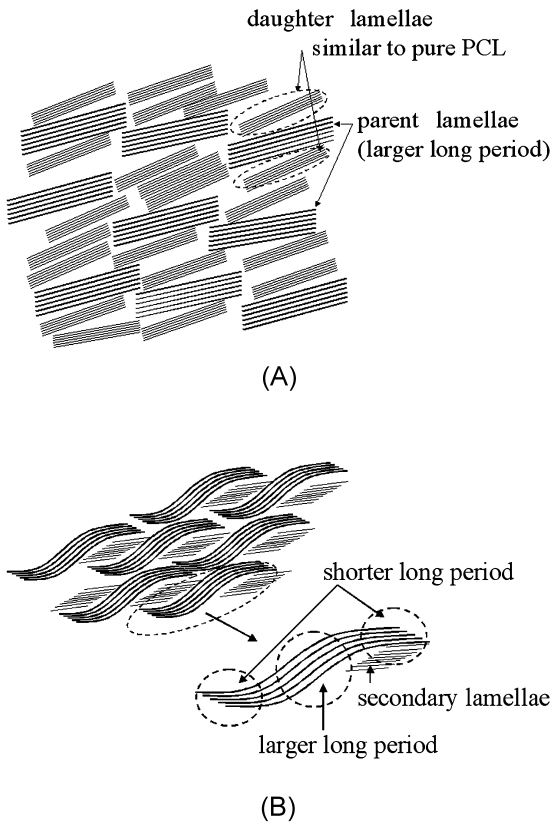

Fig. 9. The parent–daughter lamellae correlation model (A) and the S-shaped spatial distribution lamella model (B) in PCL/PVB band spherulite crystallized at 41 °C. A cross-section of lamella plane viewed from the center of the band spherulite is shown. In each model, the primary lamellae with larger long period are strongly affected by PVB, while the secondary lamellae with shorter long period are hardly affected by PVB during the crystal growth.

PCL/PVB. This S-shaped spatial distribution will be formed by the following procedure. (1) The lamellae with the larger long period, which appear in the initial stage of crystallization, laterally grow and form the S-shaped lamellae. In the central part of the S-shape, the lamellae with the larger long period are formed. On the other hand, the edge part of the S-shape which is formed by the lateral crystal growth has the lamella structure with the shorter long period. (2) When the laterally grown lamellae impinge on each other, the lamellae with the shorter long period grow by the secondary crystallization and fill the space between the main S-shaped lamellae. The growth of the secondary lamella between the primary lamellae in polyethylene was already observed by in situ AFM experiment [25] and this phenomenon is expected to occur also in PCL/PVB. With respect to the secondary lamella, the concept of the parent–daughter lamellae correlation model may be applied. For example, secondary lamellae may be the daughter lamellae which branch from that with the shorter long period near the edge part of S-shape that is priorly formed. Further, this secondary lamella may twist along the radial direction of lamella plane at the edge region of S-shape or may twist independently by the spiral growth mechanism to release

the strain from the restricted space. The characteristics of S-shaped spatial distribution model is that it can easily explain the non-parallel relation between lamella planes with the larger and shorter long periods.

In the above two models, the key point is the reason why two different kinds of lamellae appear. The origin of the appearance of two different lamella structures can be explained as follows: in the radial growth stage of primary crystallization, the PVB molecules are gathered at the radial growth front of PCL lamellae, strongly affecting the PCL lamella morphology, and form the larger long period in the primary lamella. The existence of PVB may make the crystallization growth rate slower, or PVB may be inserted into the inter-lamella region of PCL lamella, making the crystal fold surface thermally stable by the strong interaction. The effect of PVB in the formation of the larger long period is discussed later in detail. On the other hand, in the late stage of crystallization, most of PVB molecules are already taken to the radial growth front of primary lamella and the lateral or secondary crystallization of PCL may not be affected by PVB so much, resulting in the formation of lamella similar to that of pure PCL. The decrease in PVB concentration will accelerate the lateral crystallization growth rate, and the thermodynamically stable crystalline thickness becomes similar to that of pure PCL.

Our spatial distribution models described above can explain all the experimental results without contradiction. At first, the lamella planes with the larger and shorter long periods are not parallel with each other. Second, the lamella with the larger long period is formed at the initial stage of crystallization and the lamella with the shorter long period is formed later in the edge part of S-shape or in the secondary crystallization by daughter lamella. Third, the larger long periodic lamella planes that are formed at the initial stage of crystallization are preserved until the end of crystallization.

With respect to the structure of the lamellae with the larger long period, the following two possibilities can be conceived: one is that the thicker crystalline lamellae are formed with a slower crystallization velocity due to the attachment of PVB to the radial crystal growth front. This can explain the difference in the melting point between the two components of lamellae. The other possibility is that the thicker amorphous region, which includes PVB, is formed: in this case, the folded surface of crystalline lamella may be stabilized by the hydrogen bonding of PVB. This can also explain the difference in melting point between two kinds of lamellae. However, either of the two possibilities cannot be excluded from X-ray analysis alone, because SAXS analysis based on the correlation function cannot be applied to three-phase system (two kinds (larger, and shorter) of crystalline lamellae or two kinds of amorphous regions).

Regarding the PVB location in the banded spherulite, the following two possibilities can be considered in relation to the above discussion about the structure of larger lamellae: (1) PVB molecules locate in the inter-fibril region of lamella bundle (in this case, the crystalline thickness of the larger lamella is thicker than that of the shorter one). (2) They locate in the inter-lamella region of the lamella structure with the larger long period, forming thicker amorphous region.

In the case of (1), it may be considered that the exclusion of PVB to the inter-fibril region occurs in the fast twisting mode of lamella. It was previously reported that the concentration of impurity in the banded spherulite is not homogeneous but periodic along the radial direction when the growth rate of the band spherulite is step-like [26]. When the stress on the radial growth front by PVB exceeds a certain threshold value, it is released by the fast twisting mode of lamella to exclude PVB molecules from the inter-fibril region. In this case, the primary crystallization rate in the radial direction will be highly delayed by the PVB molecules which attach to the growth front, and the thicker crystal is formed.

In the case of (2), it may be considered that the interaction of the PVB molecules in the inter-lamella region with PCL is too strong to exclude PVB from the inter-lamella region of PCL.

In PCL/PVB crystallized at 41 °C, it is likely that both the above two possibilities coexist. In other words, PVB molecules gathered on the growth front are partially inserted to the inter-lamella amorphous region, and the excess PVB molecules are accumulated on the radial growth front, working as the driving force of discontinuous twisting. However, we need to perform TEM experiment to obtain the conclusion about the structure of the larger lamella and the location of PVB.

Regarding PCL/PVB crystallized at 35 °C, we cannot discuss the spatial distribution of lamella structures, because PCL/PVB crystallized at 35 °C has only one lamella structure. However, it should be noted that the angular spread of 110 lattice in WAXS simulation for PCL/PVB crystallized at 35 °C is smaller than that for PCL/PVB crystallized at 41 °C. This suggests that the distribution in orientation of lamella plane in PCL/PVB crystallized at 35 °C is smaller than that in PCL/PVB crystallized at 41 °C. It may indicate that the existence of two different long periods causes the broadening of the orientation of lamella plane in PCL/PVB crystallized at 41 °C.

Next, we will discuss the continuous twisting in PCL/PVB crystallized at 35 °C. In PCL/PVB crystallized at 35 °C, it seems that the distribution of PVB is more homogeneous in the lamella cross-section, because there exists only one lamella structure. The homogeneous PVB distribution can be explained by the following crystal growth mechanism: at lower temperature, the adjacent reentry mechanism becomes less effective [27]. In this case, the PVB molecules are no longer accumulated on the radial growth front and the homogeneous lamellae are formed. When the concentration of PVB molecules that are homogeneous on the growth front is within the capacity of inter-lamella insertion, the concentration of PVB at the radial growth front is constant during crystallization. In this

way, PVB molecules give the constant stress on the surface, resulting in the continuous twisting of lamellae.

As a future work, we should investigate the temperature dependence of (1) the degree of discontinuity in twisting (WAXS) and (2) the angle between the larger and the shorter long period planes (SAXS) in detail to discuss the formation mechanism of discontinuous twisting and the lamella inhomogeneity.

5. Conclusion

We have performed the microbeam SAXS/WAXS experiments (time-resolved SAXS during crystallization, scanning SAXS/WAXS for spatial distribution) and usual SAXS during melting. From the time-resolved microbeam SAXS and scanning microbeam SAXS experiments, we have observed that the larger lamella period appears prior to the appearance of the shorter lamella period, and that the larger and shorter lamella planes are not parallel with each other. Based on these results, we have proposed two possible spatial distribution models. Further, from microbeam scanning SAXS/WAXS combined with model simulation, we have obtained the information about the twisting manner of PCL/PVB band spherulite. Our experiments have demonstrated that the microbeam SAXS/-WAXS technique is a very powerful tool for the structural analysis of polymer blend that has μm-scale spatial distribution in its structure.

Acknowledgements

We thank Dr Kazuki ITO (Stanford University) and Dr Hironari KAMIKUBO (NAIST, Japan) for their help in our experiments performed at Photon Factory. This work has been performed under the approval of the Photon Factory Program Advisory Committee (Proposal No. 00G057).

References

[1] Chiu HJ, Chen HL, Lin TL, Lin JS. Macromolecules 1999;32:4969.
[2] Chen HL, Hwang JC, Yang JM, Wang RC. Polymer 1998;39:6983.
[3] Wang Z, An L, Jiang W, Jiang B, Wang X. J Polym Sci, Polym Phys 1999;37:2682.
[4] Hobbs JK, Binger DR, Keller A, Barham PJ. J Polym Sci, Polym Phys 2000;38:1575.
[5] Riekel C, Engstroem P, Martin C. J Macromol Sci, Phys 1998;B37: 587.
[6] Waigh TA, Donald AM, Heidelbach F, Riekel C, Gidley MJ. Biopolymers 1999;49:91.
[7] Dreher S, Zachmann HG, Riekel C, Engstroem P. Macromolecules 1995;28:7071.
[8] Riekel C, Cedola A, Heidelbach F, Wagner K. Macromolecules 1997; 30:1033.
[9] Mueller M, Riekel C, Vuong R, Chanzy H. Polymer 2000;41:2627.
[10] Kolb R, Wutz C, Stribeck N, von Krosigk G, Riekel C. Polymer 2001; 42:5257.
[11] Keith HD, Padden FJ, Russel TP. Macromolecules 1989;22:666.
[12] Lee JC, Nakajima K, Ikehara T, Nishi T. J Appl Polym Sci 1997;64: 797.
[13] Iida A, Noma T. Nucl Instrum Methods 1993;B82:129.
[14] Blanton TN, Barnes CL, Lelental M. J Appl Crystallogr 2000;33:172.
[15] Amemiya Y, Ito K, Yagi N, Asano Y, Wakabayashi K, Ueki T, Endo T. Rev Sci Instrum 1995;66:2290.
[16] Amemiya Y, Wakabayashi K, Hamanaka T, Wakabayashi T, Matsushita T, Hashizume H. Nucl Instrum Methods 1983;208:471.
[17] Chatani Y, Okita Y, Tadokoro H, Yamashita Y. Polym J 1970;1:555.
[18] Ryan AJ, Stanford JL, Bras W, Nye TMW. Polymer 1997;38:759.
[19] Keller A. J Polym Sci 1955;17:351.
[20] Fujiwara Y. J Appl Polym Sci 1960;4:10.
[21] Bassett DC. Principles of polymer morphology. Cambridge, UK: Cambridge University Press; 1981. p. 61.
[22] Keith HD, Padden FJ. Macromolecules 1996;29:7776.
[23] Keith HD, Padden FJ. Polymer 1984;25:28.
[24] Ho RM, Ke KZ, Chen M. Macromolecules 2000;33:7529.
[25] Hobbs JK, Winkel AK, McMaster TJ, Humphris ADL, Baker AA, Blakely S, Aissaoui M, Miles MJ. Macromol Symp 2001;167:1.
[26] Kyu T, Chiu HW, Gruenthner AJ, Okabe Y, Saito H, Inoue T. Phys Rev Lett 1999;83:2749.
[27] Hoffman JD, Frolen LJ, Gaylon SR, Lauritzen JI. J Res Nat Bur Stand (US) 1975;79A:671.